

# IONORT: a Windows software tool to calculate the HF ray tracing in the ionosphere

A. Azzarone, C. Bianchi, M. Pezzopane\*, M. Pietrella, C. Scotto, A. Settimi

*Istituto Nazionale di Geofisica e Vulcanologia, Via di Vigna Murata, 605, 00143 Rome, Italy*

michael.pezzopane@ingv.it

Tel.: +390651860525

Fax: +390651860397

## **Abstract**

This paper describes an applicative software tool, named IONORT (IONOspheric Ray Tracing), for calculating a three-dimensional ray tracing of high frequency waves in the ionospheric medium. This tool runs under Windows operating systems and its friendly graphical user interface facilitates both the numerical data input/output and the two/three-dimensional visualization of the ray path. In order to calculate the coordinates of the ray and the three components of the wave vector along the path as dependent variables, the core of the program solves a system of six first order differential equations, the group path being the independent variable of integration. IONORT uses a three-dimensional electron density specification of the ionosphere, as well as by geomagnetic field and neutral particles-electrons collision frequency models having validity in the area of interest.

Keywords: ray tracing, ray path, ionospheric models.

25 **1. Introduction**

26 Ray tracing (RT) is a numerical technique used to determine the path of a high frequency (HF)  
27 radio wave in anisotropic and inhomogeneous media different from the vacuum (Budden, 1988).  
28 The technique works properly if the refractive index is assumed to be known in each point of the  
29 considered region. In the limits of the ray theory it is possible to approximate the wavelength to  
30 zero, simplifying consequently the differential equations describing the propagation of the wave in a  
31 suitable way, i.e. the ray path. Hence, three-dimensional (3-D) RT algorithms calculate the  
32 coordinates reached by the wave vector and its three components, the group time delay of the wave  
33 along the path and other optional quantities (geometrical and phase path, absorption, polarization,  
34 etc.). In order to accomplish these tasks, the RT programs integrate at least six differential  
35 equations, plus other equations when additional quantities, like for instance Doppler frequency  
36 shift, are required. These kinds of algorithms were developed in the 1950's (Haselgrove, 1955;  
37 Duziak, 1961; Croft and Gregory, 1963) for old mainframes that were able to give only a numerical  
38 output. Nowadays, these programs have been optimized and adapted to Over The Horizon radar  
39 applications (Coleman, 1998; Nickish, 2008) by using powerful computers and devices for a real-  
40 time use.

41 This paper deals with a software tool, named IONORT, whose RT algorithm is based on a system  
42 of first order differential equations with Hamiltonian formalism that are solved for a geocentric  
43 spherical coordinate system. The corresponding software (that can be downloaded at the site  
44 [ftp://ftp.ingv.it/pub/adriano.azzarone/ionort\\_0.7.2.zip](ftp://ftp.ingv.it/pub/adriano.azzarone/ionort_0.7.2.zip)) is written in MATLAB for the input and the  
45 output routines, while the integration algorithm is derived from the one that was coded in Fortran by  
46 Jones and Stephenson (1974). In the next future, a whole package coded in MATLAB is planned.  
47 The ionosphere considered by this software tool is represented by 3-D ionospheric regional models  
48 elaborated at the Istituto Nazionale di Geofisica e Vulcanologia. An analytical standard Chapman  
49 modeled ionosphere (Chapman, 1931) useful mainly for test purpose complete the whole package.

50

## 51 2. Generality on the ionospheric ray tracing algorithm

52 Ray tracing techniques rely on a comprehensive specification of the ionosphere in terms of  
53 electron density, neutral particles-electrons collision frequency, and geomagnetic field. As an  
54 example, Fig. 1 shows a 3-D matrix of the electron density where in each cell  $C_{ijk}$  (here, the indexes  
55  $i, j,$  and  $k$  are respectively the longitude, the latitude, and the altitude and these depend on the  
56 corresponding matrix resolution) the electron density of the ionospheric medium, and hence the  
57 corresponding complex refractive index  $n$ , has a defined value.

58 Fig. 1 shows also a possible ray path from a transmitting (TX) point to a receiving (RX) point  
59 across the cells of the 3-D electron density matrix with the frequency and direction of the wave, and  
60 the position of the TX point given as input. The RT algorithm integrates the following partial  
61 differential equations

62

$$63 \quad \frac{d r_i}{d \tau} = \frac{\partial H(r_i, k_i)}{\partial k_i} \quad (1.1)$$

64

$$65 \quad \frac{d k_i}{d \tau} = \frac{\partial H(r_i, k_i)}{\partial r_i} \quad (1.2)$$

66

67 where  $i=1, \dots, 4$ ,  $H(r_i, k_i)$  is the Hamiltonian,  $r_i$ , and  $k_i$ , are respectively the generalized coordinates  
68 and momenta, while the independent variable  $\tau$  must be a monotonic increasing quantity  
69 (represented in our case by the group path) (Weinberg, 1962). (1.1) and (1.2) are solved for a  
70 geocentric spherical coordinate system  $(r, \theta, \varphi)$ , and according to the wave vector components, as  
71 shown in Fig. 2 (Bianchi and Bianchi, 2009; Bianchi et al., 2010). The essential differential  
72 equations that are integrated are given more explicitly in the Appendix A.

73

74

75 **3. IONORT: description of the program**

76 IONORT is structured in three main blocks:

77

78 a) INPUT GRAPHICAL USER INTERFACE;

79 b) INTEGRATION ALGORITHM;

80 c) OUTPUT GRAPHICAL USER INTERFACE.

81

82 Fig. 3 shows the flowchart of the IONORT application.

83 The block a), developed in MATLAB, firstly reads a file named “DATA\_default.ini” to initialize  
84 the default inputs related to all the computational parameters needed by the ray-tracing algorithm.

85 After this phase of initialization, it visualizes a graphical user interface (GUI, see Fig. 4 or Fig. 5)

86 by which the user can modify the default inputs, and then it generates a file “DATA\_in.txt”

87 representing the user input for the integration executable code, written in Fortran, that is the block

88 b). “DATA\_in.txt” is then nothing but a copy of the file “DATA\_default.ini” modified according to

89 the choices made by the user. “DATA\_in.txt” is then the actual input of the Fortran core, which

90 reads it as a vector  $W$  of 400 components. Table 1 shows the first 25 components of such a vector,

91 in particular: the geographical coordinates of the TX point, the height (in km) of the TX and the RX

92 points at which the program must start and stop respectively, the azimuth and elevation angles (in

93 degrees), the wave operating frequency (in MHz), the polarization of the ray (ordinary or

94 extraordinary), the geographical coordinates of the geomagnetic pole, the number of hops, and some

95 needed constants like for instance the Earth radius. The user can modify some of these input

96 parameters, as well as the analytical or numerical models representing the ionosphere (according to

97 what is shown by Table 2), by filling and checking the corresponding boxes of the “Main

98 parameters”, “Step”, “Model”, and “Ray” frames of the GUI. Once the parameters have been set,

99 the “RUN” button launches the integration algorithm.

100 The block b), which is the core of the application, is represented by this integration algorithm that  
101 is coded as a Fortran executable. In order to integrate step by step the differential equations  
102 illustrated in the Appendix A, this executable performs all the computational operations using either  
103 the 4-order Runge-Kutta (RK) method (Press et al., 1996) or the Adams-Bushford predictor and the  
104 Adams-Moulton corrector methods (ABAM) (Press et al., 1996). Using these, the ray path of the  
105 wave in spherical coordinates is calculated.

106 Once this task ended, the block c), besides saving the numerical output in a file “RToutput.txt”,  
107 visualizes the results in the GUI where also 2-D and 3-D graphical elaborations of the ray path are  
108 performed. The 2-D visualization is plotted at the bottom of the GUI in a plane section having  
109 constant azimuth. The 3-D visualization is plotted on the right side of the GUI. The numerical  
110 output of some relevant parameters like the latitude and the longitude of the arrival point, the  
111 ground range distance on the Earth’s surface, the maximum altitude of the path trajectory (apogee),  
112 and the time delay of the ray along the whole path (group delay) are shown in the “Results” frame  
113 of the GUI.

114 IONORT can run both with a fixed operating frequency and with a frequency-step procedure. The  
115 same is for the elevation and the azimuth angles. Fig. 4 and Fig. 5 show two examples of  
116 elaboration, by taking into account a TX point at 43.06°N of latitude and at 10.03°E of longitude,  
117 the former for a fixed frequency equal to 6 MHz and for a 5° elevation-step procedure from 0° to  
118 30°, the latter for a fixed elevation angle equal to 15° and for a 2 MHz frequency-step procedure  
119 from 2 MHz to 24 MHz.

120

#### 121 **4. Description of the integration computational code**

122 The main task of IONORT is the integration of the first-order differential equation system given in  
123 the Appendix A. The discrete form of the system can be write as

124

125 
$$\frac{d y_i}{d \tau} = f_i(\tau, y_1, \dots, y_N), \quad (2)$$

126

127 where  $i=1, \dots, N$ ,  $y_i$  are the dependent variables (coordinates and wave vector components) and  $\tau$  is  
 128 the independent variable. For each of the six equations of the system, at the step  $n+1$  the classical 4-  
 129 order RK formula gives

130

131 
$$y_{n+1} = y_n + h \frac{1}{6} (k_1 + 2k_2 + 2k_3 + k_4), \quad (3.1)$$

132

133 with

134 
$$\tau_{n+1} = \tau_n + h, \quad (3.2)$$

135

136 where  $n$  and  $h$  represent respectively the integration step number and the integration step value,  
 137  $k_1=f(\tau_n, y_n)$ ,  $k_2=f(\tau_n+h/2, y_n+hk_1/2)$ ,  $k_3=f(\tau_n+h/2, y_n+hk_2/2)$ , and  $k_4=f(\tau_n+h, y_n+hk_3)$ . Alternatively, the  
 138 system can be solved using the ABAM method. In the RK method the independent variable  $\tau$  can  
 139 assume values from tens of meters to a few kilometers, while in the ABAM method there is an  
 140 adaptive step according with a maximum and a minimum tolerated error.

141 With regard to the refractive index calculation routine, as we have already mentioned in the  
 142 paragraph 3, besides the possibility of considering an analytical standard Chapman modeled  
 143 ionosphere (Chapman, 1931), numerical representations of the ionosphere can also be considered.  
 144 The corresponding 3-D electron density matrixes (as the one shown in Fig. 1) are formed by cells  
 145 extending tens of kilometers in latitude and in longitude, and a few kilometers in altitude. At each  
 146 step of integration the algorithm evaluates the actual cell  $C_{ijk}$  along the path, according to the  
 147 flowchart shown in Fig. 6, and hence takes the corresponding value of electron density, which is  
 148 considered the same inside the whole cell.

149 Concerning the numerical 3-D representation of the ionosphere, this is based either on the  
150 Adaptive Ionospheric Profiler (AIP) model developed by Scotto (2009) or on the model proposed  
151 by Pezzopane et al. (2011). Both models derive from the International Reference Ionosphere  
152 (Bilitza, 2008) and rely on the real-time autoscaling performed both by Autoscala (Pezzopane and  
153 Scotto, 2007, 2008, 2010) and by ARTIST (Reinisch and Huang, 1983, Galkin and Reinisch, 2008).  
154

## 155 **5. Consistency check of the integration algorithm**

156 In order to check the error due to the integration algorithm, the time delay of the wave as it results  
157 from the RT computation performed by IONORT, and the time delay of the wave propagating along  
158 the oblique virtual path at the speed of light  $c$ , were compared at different frequencies. In order to  
159 calculate the latter time delay, a flat reflector is assumed at an altitude compatible with the vertical  
160 virtual height of reflection. The relation between the vertical and oblique frequencies is given by the  
161 secant law  $f_v = f_{ob} \cos \varphi$  (Davies, 1990), where  $\varphi$  is the incidence angle,  $f_v$  is the vertical frequency,  
162 and  $f_{ob}$  is the oblique frequency. The equality of the two time delays is assured by the Breit-Tuве  
163 and Martyn theorems (Davies, 1990) in case of a monotonically increasing electron density profile.  
164 Bianchi et al. (2011) ran such a test by employing a numerical electron density matrix, and the  
165 corresponding results are shown in Fig. 7. It came out that the IONORT ray tracing algorithm fits  
166 nearly perfectly the theory stated by the two aforementioned theorems. This means that the relative  
167 error  $\Delta t_{\text{error}}$  between the time delay  $t_{\text{calc}}$  calculated by IONORT and the simulated time delay  $t_{\text{virt}}$ ,  
168 calculated according to the Breit-Tuве and Martyn theorems, is only due to the discrete integration  
169 step.

170

## 171 **6. Conclusions**

172 In this paper, an applicative software tool package running under Windows operating system,  
173 named IONORT, capable to solve the ray tracing for HF waves propagating in the ionosphere was  
174 described. The integration algorithm of IONORT is coded in Fortran, while the GUI managing the

175 input needed to the integration algorithm, and the corresponding numerical and graphical output, is  
176 coded in MATLAB. This GUI facilitates noticeably the numerical input data entry made by the user  
177 and at the same time performs a useful 2-D/3-D visualization of the ray path.

178 From a numerical point of view, in order to calculate the coordinates of the ray and the three wave  
179 vector components along the path as dependent variables, IONORT solves at least six first order  
180 differential equations, the group time being the independent variable of integration.

181 The consistency of the integration algorithm was checked by comparing real and virtual time  
182 delays.

183 The possibility offered to the user of choosing among different ionospheric electron density  
184 models, having validity in the area of interest, gives IONORT the necessary flexibility. It is worth  
185 noting that this last feature makes IONORT a valuable tool to test the goodness of the 3-D electron  
186 density representation of the ionosphere calculated by a definite model. In fact, given a radio link  
187 for which oblique soundings are routinely carried out, IONORT gives the possibility to generate  
188 synthesized oblique ionograms over the same radio link. The comparison between synthesized and  
189 measured oblique ionograms, both in terms of the ionogram shape and in terms of the maximum  
190 usable frequency characterizing the radio path, offers a great opportunity to understand how well  
191 the model can represent the real conditions of the ionosphere (Angling and Khattatov, 2006).  
192 Anyhow, this issue will be presented and discussed in a forthcoming paper.

193

#### 194 **Appendix A. Equation (1.1) and (1.2) in spherical coordinates**

195 In spherical coordinates the equations (1.1) and (1.2) become

196

$$197 \quad \frac{dr}{d\tau} = \frac{\partial H}{\partial k_r}, \quad (\text{A.1})$$

198



199 
$$\frac{d\theta}{d\tau} = \frac{1}{r} \frac{\partial H}{\partial k_\theta}, \quad (\text{A.2})$$

200

201 
$$\frac{d\varphi}{d\tau} = \frac{1}{r \sin \theta} \frac{\partial H}{\partial k_\varphi}, \quad (\text{A.3})$$

202

203 
$$\frac{dk_r}{d\tau} = -\frac{\partial H}{\partial r} + k_\theta \frac{d\theta}{d\tau} + k_\varphi \sin \theta \frac{d\varphi}{d\tau}, \quad (\text{A.4})$$

204

205 
$$\frac{dk_\theta}{d\tau} = -\frac{1}{r} \left( -\frac{\partial H}{\partial \theta} - k_\theta \frac{dr}{d\tau} + k_\varphi r \cos \theta \frac{d\varphi}{d\tau} \right), \quad (\text{A.5})$$

206

207 
$$\frac{dk_\varphi}{d\tau} = -\frac{1}{r \sin \theta} \left( -\frac{\partial H}{\partial \varphi} - k_\varphi \sin \theta \frac{dr}{d\tau} - k_\theta r \cos \theta \frac{d\theta}{d\tau} \right), \quad (\text{A.6})$$

208

209 where  $H$  is the Hamiltonian,  $k_r$ ,  $k_\theta$ ,  $k_\varphi$  (see Fig. 2) are the components of the wave vector along  $r$ ,  $\theta$ ,  
 210 and  $\varphi$ . The Hamiltonian  $H$  is a constant during the ray propagation, and for the IONORT algorithm  
 211 the following relation was chosen

212

213 
$$H(r, \theta, \varphi, k_r, k_\theta, k_\varphi) = \frac{1}{2} \text{Re} \left[ \frac{c^2}{\omega^2} (k_r^2 + k_\theta^2 + k_\varphi^2) - n^2 \right], \quad (\text{A.7})$$

214

215 where  $n$  is the phase refractive index,  $c$  is the speed of light, and  $\omega$  is the fixed angular frequency of  
 216 the wave.

217

218 **References**

219 Angling, M. J., Khattatov, B., 2006. Comparative study of two assimilative models of the  
220 ionosphere, *Radio Science*, 41, RS5S20, doi:10.1029/2005RS003372.

221

222 Bianchi, C., Bianchi, S., 2009. Problema generale del ray-tracing nella propagazione ionosferica –  
223 formulazione della ray theory e metodo del ray-tracing. INGV Technical Report N. 104, INGV  
224 Printing Office, Rome, Italy, 26 pp. [in Italian].

225

226 Bianchi, C., Settimi, A., Azzarone, A., 2010. IONORT - Ionosphere Ray-Tracing (Programma di  
227 ray-tracing nel magnetoplasma ionosferico). INGV Technical Report N. 161, INGV Printing Office,  
228 Rome, Italy, 20 pp. [in Italian].

229

230 Bianchi, C., Settimi, A., Scotto, C., Azzarone, A., Lozito, A., 2011. A method to test HF ray tracing  
231 algorithm in the ionosphere by means of the virtual time delay. *Advances in Space Research*,  
232 48(10), 1600–1605.

233

234 Bilitza, D., Reinisch, B.W., 2008. International Reference Ionosphere 2007: Improvements and new  
235 parameters. *Advances in Space Research*, 42(4), 599–609, doi:10.1016/j.asr.2007.07.048.

236

237 Budden, K.G., 1988. *The propagation of the radio wave*. Cambridge University Press, Cambridge,  
238 UK, 688 pp.

239

240 Chapman, S., 1931. The absorption and dissociative or ionizing effect of monochromatic radiation  
241 in an atmosphere on a rotating earth, *Proceedings of the Physical Society of London*, 43 (1), 26-45.

242

243 Coleman, C. J., 1998. A ray-tracing formulation and its application to some problems in over-the-  
244 horizon radar. *Radio Science*, 33 (4), 1187-1197.  
245

246 Croft, T. A., Gregory, L., 1963. A fast, versatile ray-tracing program for IBM 7090 digital  
247 computers. Rept. SEL-63-107, TR 82, contract No. 225 (64), Stanford University, Stanford  
248 Electronics Laboratories, Office of Naval Research, Advanced Research Projects Agency,  
249 Standford, California, USA, 23 pp.  
250

251 Davies, K., 1990. *Ionospheric Radio*. Peter Peregrinus Ltd., London, UK, 508 pp.  
252

253 Duziak, W. F., 1961. Three-Dimensional ray trace computer program for electromagnetic wave  
254 propagation studies. Technical Report, DASA 1232, RM 61 TMP-32, Santa Barbara, California,  
255 USA, 179 pp.  
256

257 Galkin, I. A., Reinisch, B.W., 2008. The new ARTIST 5 for all Digisondes. *Ionosonde Network*  
258 *Advisory Group Bulletin* 69, pp. 1–8, IPS Radio and Space Serv., Surry Hills, N. S. W., Australia.  
259 [Available at <http://www.ips.gov.au/IPSHosted/INAG/web-69/2008/artist5-inag.pdf>.]  
260

261 Haselgrove, J., 1955. Ray theory and new method for ray-tracing. Report of the Physical Society  
262 Conference, pp. 355-364, The Physical Society, London, UK.  
263

264 Jones, R. M., Stephenson, J. J., 1975. A versatile three-dimensional ray tracing computer program  
265 for radio waves in the ionosphere. OT Report, 75-76, U. S. Department of Commerce, Office of  
266 Telecommunication, U. S. Government Printing Office, Washington, USA, 185 pp.  
267

268 Nickish, L.J., 2008. Practical application of Haselgrove's equation for HF systems. Radio Scientific  
269 Bulletin URSI N.325, 36-48.  
270

271 Pezzopane, M., Pietrella, M., Pignatelli, A., Zolesi, B., Cander, L.R., 2011. Assimilation of  
272 autoscaled data and regional and local ionospheric models as input sources for real-time 3-D  
273 International Reference Ionosphere modeling, Radio Science, 46, RS5009,  
274 doi:10.1029/2011RS004697.  
275

276 Pezzopane, M., Scotto, C., 2007. Automatic scaling of critical frequency foF2 and MUF(3000)F2:  
277 A comparison between Autoscala and ARTIST 4.5 on Rome data. Radio Science, 42, RS4003,  
278 doi:10.1029/2006RS003581.  
279

280 Pezzopane, M., Scotto, C., 2008. A method for automatic scaling of F1 critical frequencies from  
281 ionograms. Radio Science, 43, RS2S91, doi:10.1029/2007RS003723.  
282

283 Pezzopane, M., Scotto, C., 2010. Highlighting the F2 trace on an ionogram to improve Autoscala  
284 performance. Computer & Geosciences, 36, 1168-1177, doi:10.1016/j.cageo.2010.01.010.  
285

286 Press, W.H., Teukolsky, W.T., Vetterling, B.P., Flannery, S.A., 1996. Numerical Recipes in Fortran  
287 90: The Art of Parallel Scientific Computing. Volume 2 of Fortran Numerical Recipes, Second  
288 Edition, Cambridge University Press, UK.  
289

290 Reinisch, B.W., Huang, X., 1983. Automatic calculation of electron density profiles from digital  
291 ionograms: 3. Processing of bottom side ionograms. Radio Science, 18(3),  
292 doi:10.1029/RS018i003p00477.  
293

294 Scotto, C., 2009. Electron density profile calculation technique for Autoscala ionogram analysis.  
295 Advances in Space Research, doi:10.1016/j.asr.2009.04.037.  
296  
297 Weinberg, S., 1962. Eikonal Method in Magnetohydrodynamics. The Physical Review, 126(6),  
298 1899-1909.  
299

300 **Fig. 1.** 3-D matrix of the electron density, where  $i$  and  $j$  vary with the latitude and longitude, and  $k$   
301 with the altitude, respectively. Column on the left composed by  $k$  cells represents the vertical  
302 electron density profile  $V_{ij}$ . Ray path from a TX point to a RX point is represented by a dotted  
303 curve. Because of the involved distance, the 3-D matrix has a spherical shell shape.

304

305 **Fig. 2.** Geocentric reference system in spherical  $(r, \theta, \varphi)$  and Cartesian  $(x, y, z)$  coordinates.  $\mathbf{k}$  is the  
306 wave vector and in red, in blue and in violet the corresponding projections along versors  $i_r$ ,  $i_\theta$ , and  
307  $i_\varphi$ .

308

309 **Fig. 3.** Flowchart of IONORT application.

310

311 **Fig. 4.** GUI of IONORT program. “Main parameters” and “Step” frames are related to the input  
312 data. “Model” frame shows the analytical and numerical ionospheric models that can be chosen by  
313 the user. “Ray” frame gives the user the possibility to choose between the two different polarization  
314 of the wave, ordinary or extraordinary. “Results” frame shows the numerical output values. “RUN”  
315 button launches the integration algorithm. “Reset” button clears all the different outputs. At the  
316 bottom and on the right side, the 2-D and the 3-D visualizations of the ray path are respectively  
317 shown by considering a TX point at  $43.06^\circ\text{N}$  of latitude and at  $10.03^\circ\text{E}$  of longitude, for a fixed  
318 frequency equal to 6 MHz and for a  $5^\circ$  elevation-step procedure from  $0^\circ$  to  $30^\circ$ .

319

320 **Fig. 5.** Same as Fig. 3 for a fixed elevation angle equal to  $15^\circ$  and for a 2 MHz frequency-step  
321 procedure from 2 MHz to 24 MHz.

322

323 **Fig. 6.** Flowchart of subroutine “cellfind”.

324

325 **Fig. 7.** Time group delays,  $t_{\text{virt}}$  and  $t_{\text{calc}}$ , calculated by employing a numerical electron density  
326 matrix, and corresponding percentage relative error.

327

328 **Table 1.** First 25 components of the input vector  $W$ .

329

330 **Table 2.** Analytical and numerical electron density models that can be used by IONORT. NF and  
331 WF stand for no magnetic field and with magnetic field respectively. Because of the ray path does  
332 not change significantly at the employed operating frequencies, the models do not include the  
333 neutral particles-electrons collision frequency.

Figure 1  
[Click here to download high resolution image](#)

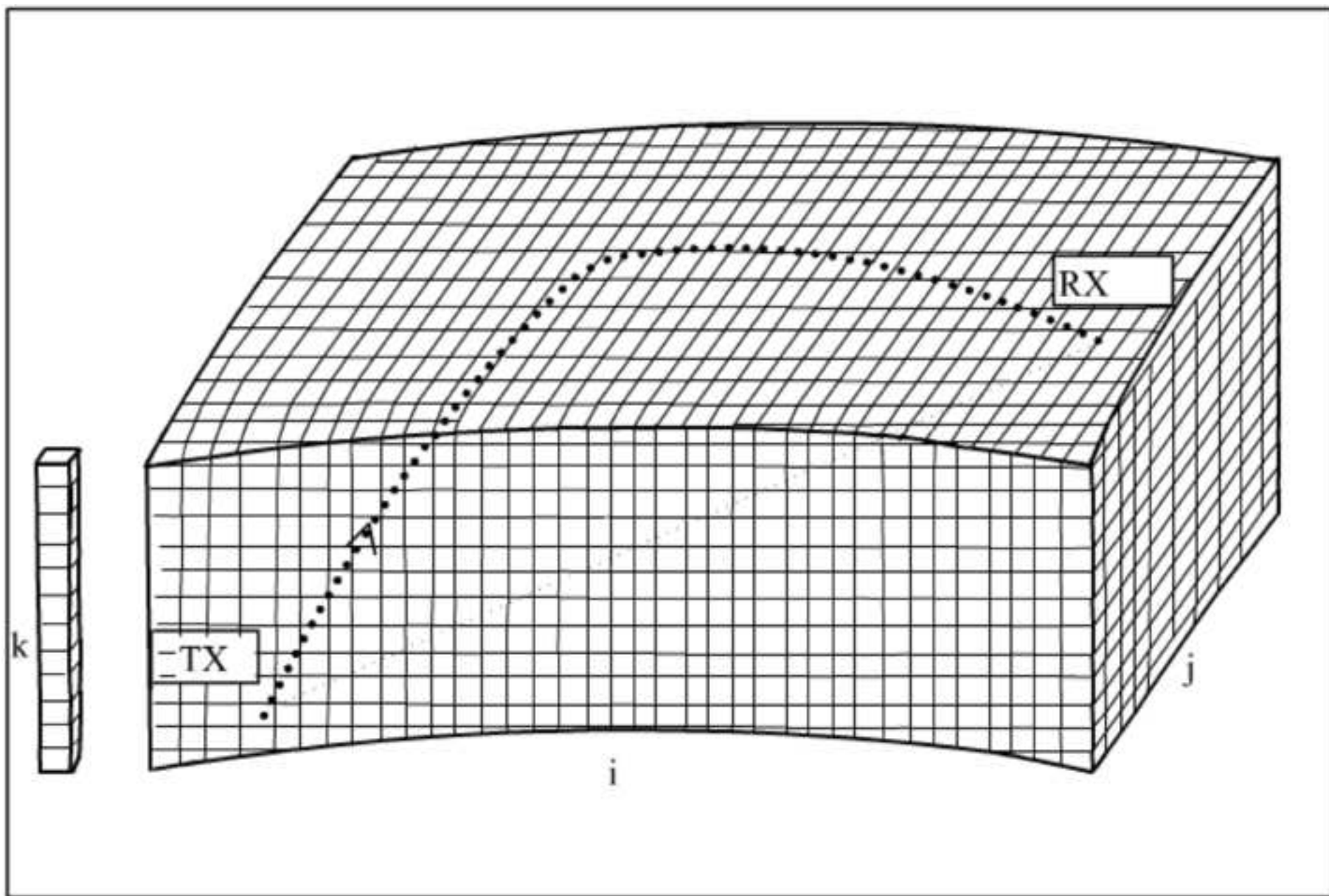




Figure 2  
[Click here to download high resolution image](#)

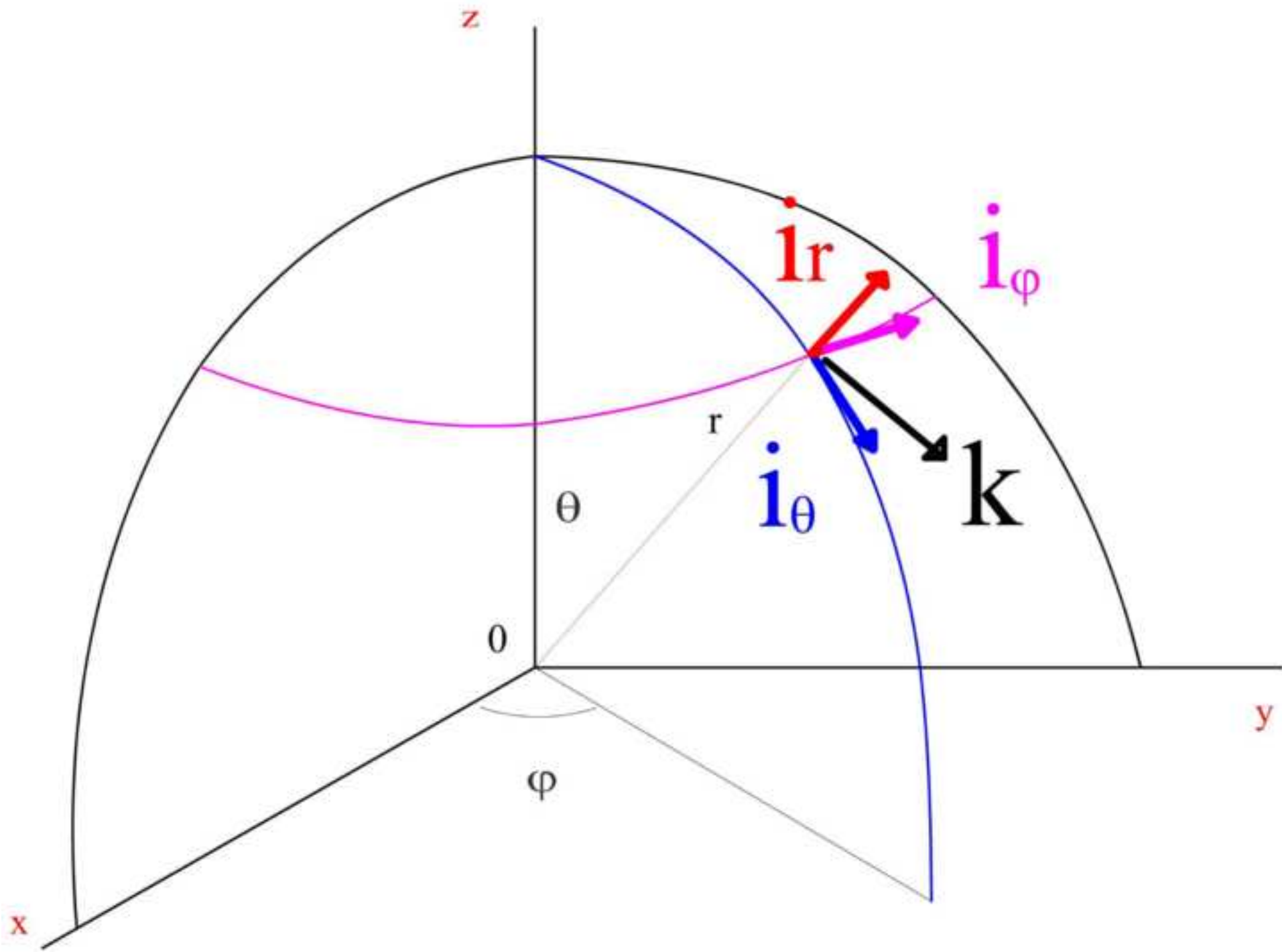


Figure 3  
[Click here to download high resolution image](#)

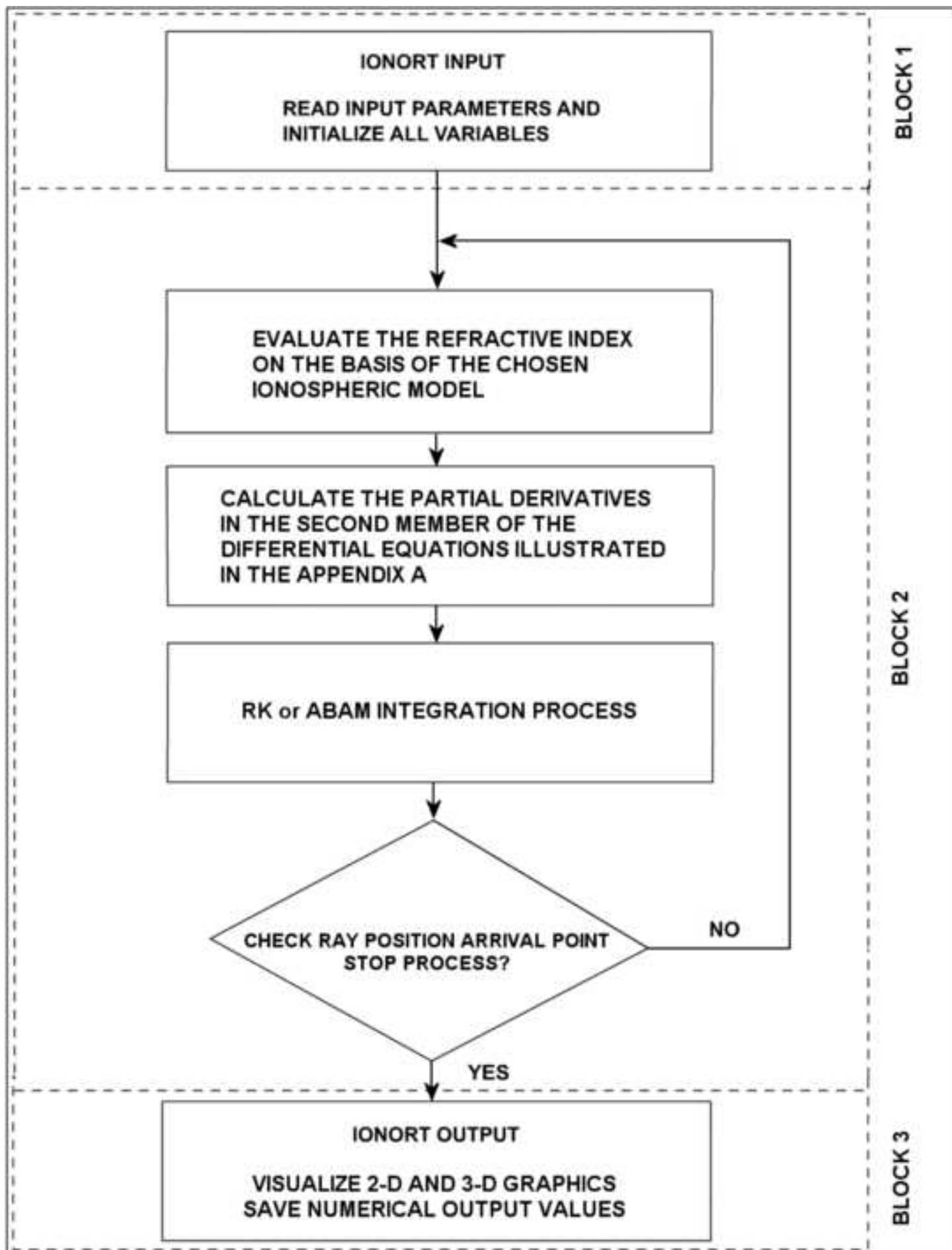


Figure 4  
[Click here to download high resolution image](#)

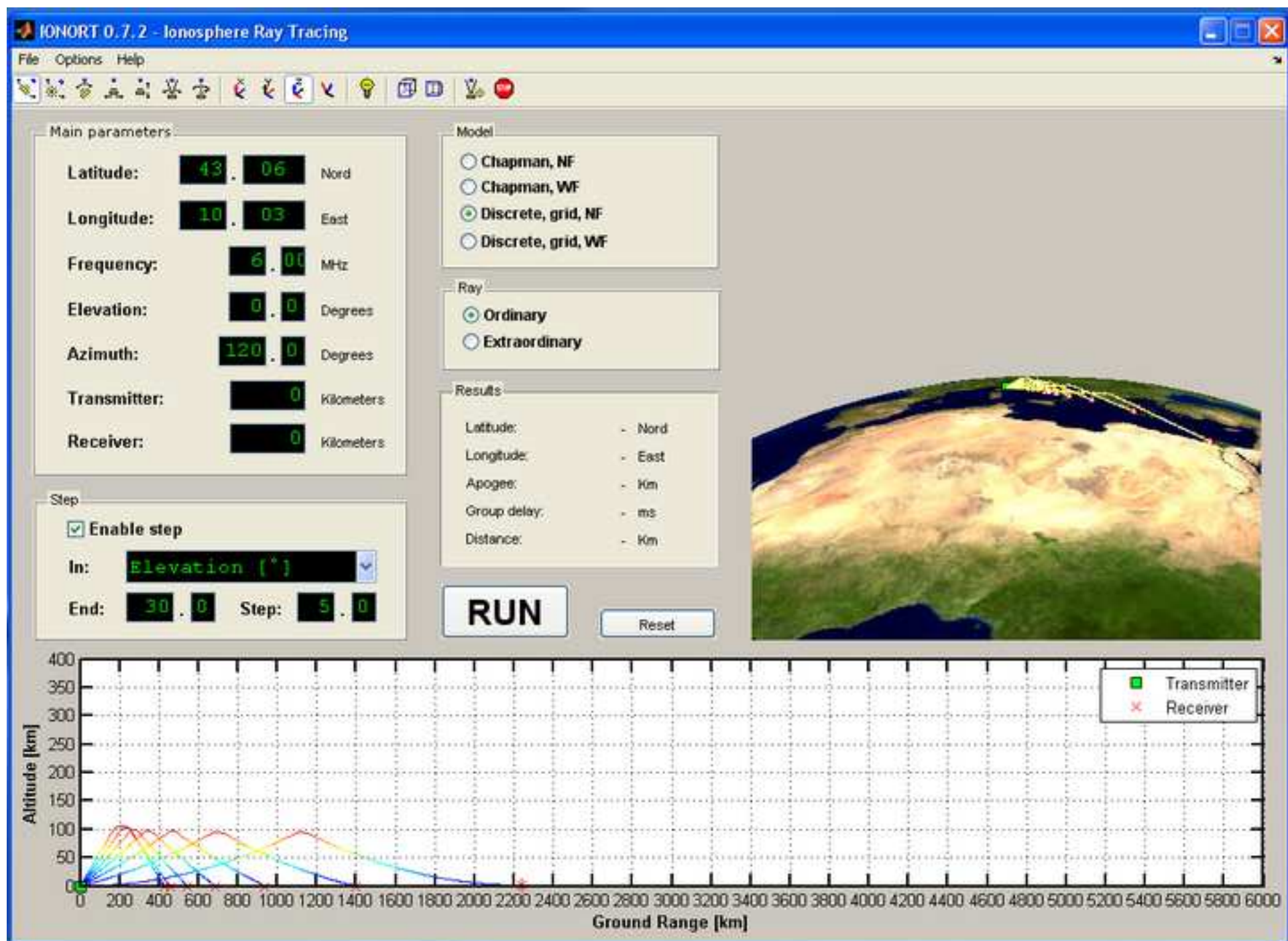


Figure 5  
[Click here to download high resolution image](#)

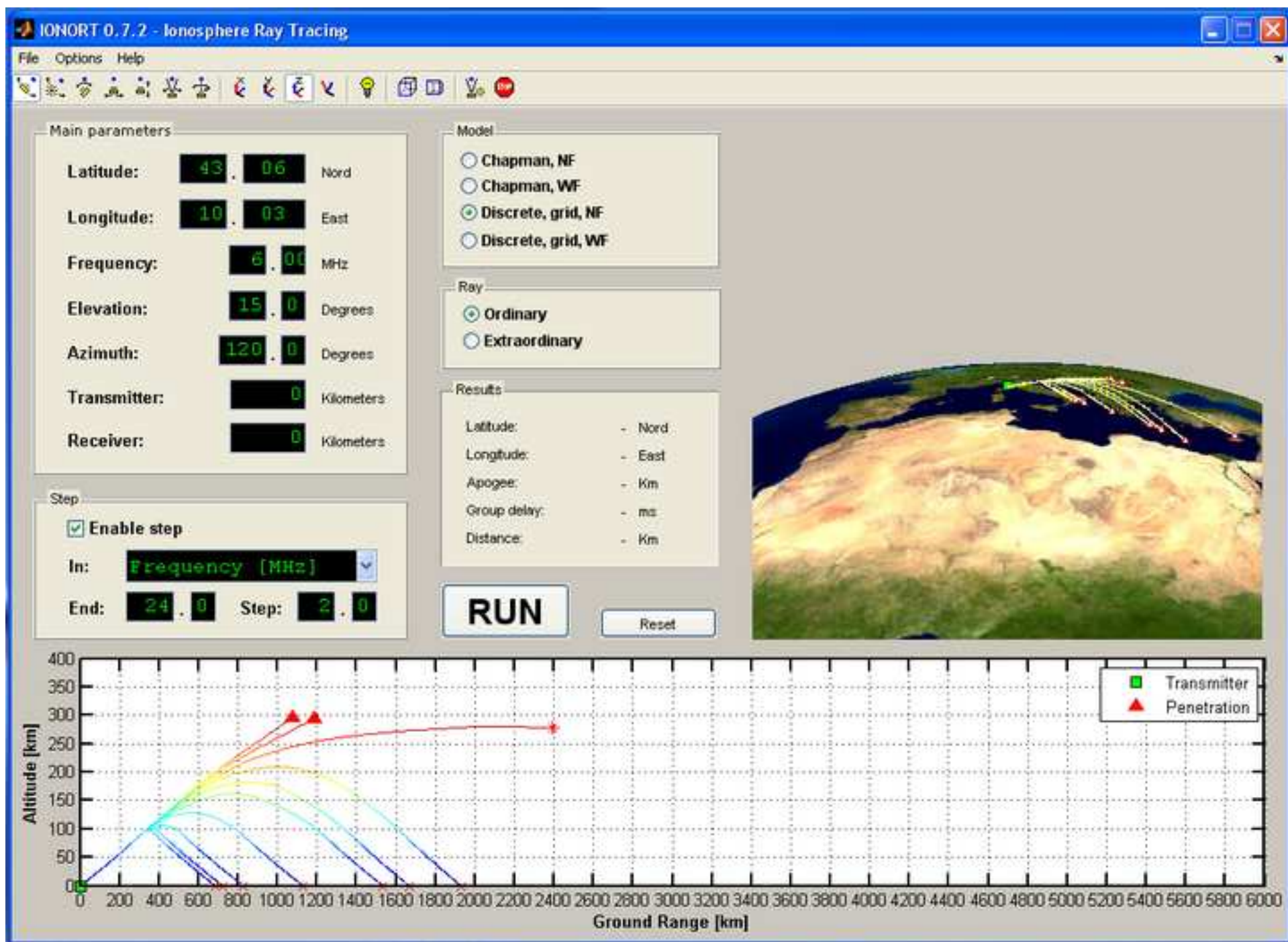


Figure 6

[Click here to download high resolution image](#)

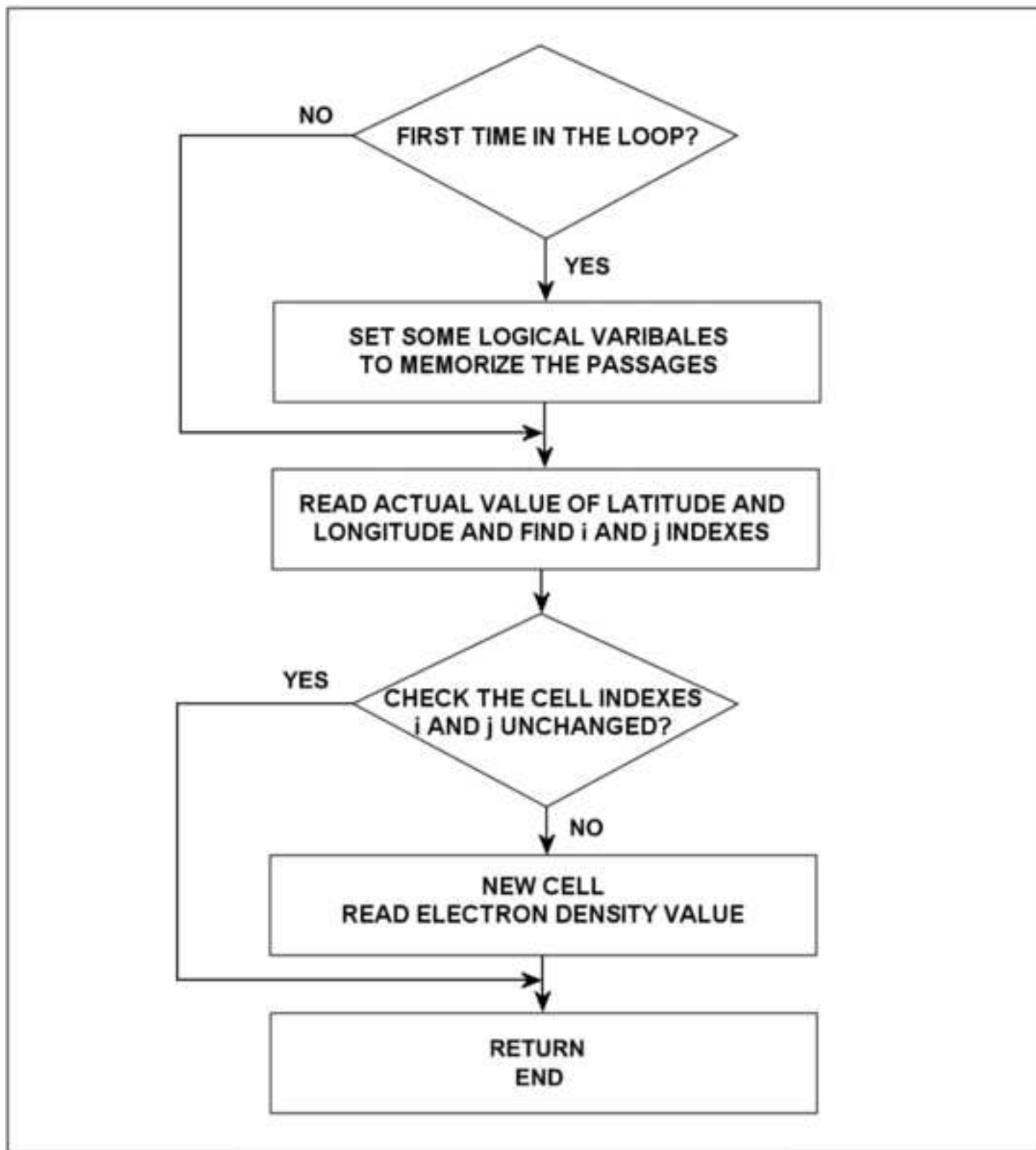


Figure 7

[Click here to download high resolution image](#)

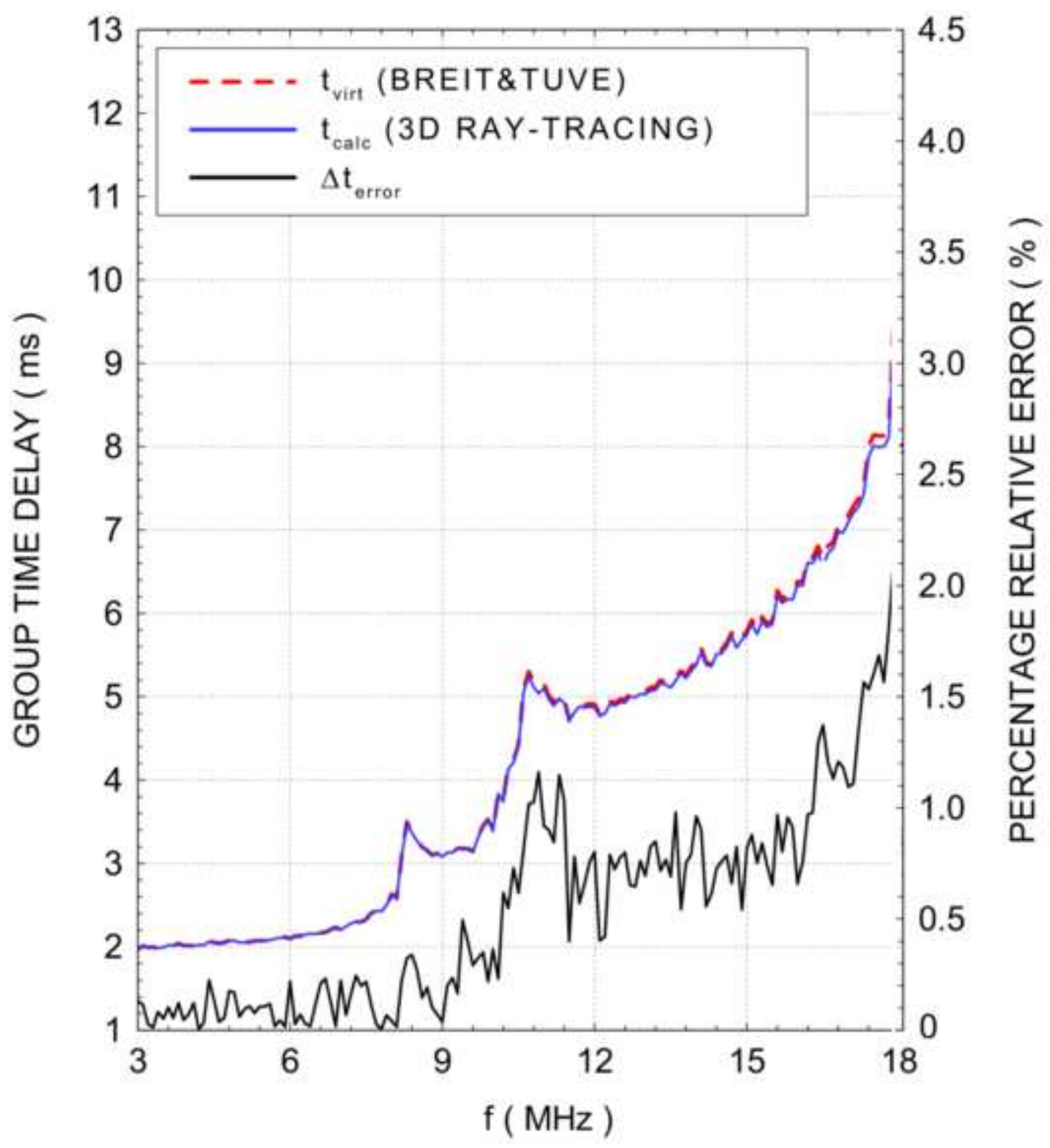


Table 1

<b>W vector component</b>	<b>Parameter</b>	<b>Description</b>	<b>Value</b>
W1	<b>RAY</b>	Radio Wave Mode	1 = Ordinary -1 = Extraordinary
W2	<b>EARTH</b>	Earth Radius	6371 km
W3	<b>XMTRH</b>	Height of TX	km
W4	<b>TLAT</b>	North geographic latitude of TX	rad
W5	<b>TLON</b>	East geographic latitude of TX	rad
W6	<b>F</b>	Frequency	MHz
W7	<b>FBEG</b>	Initial frequency	MHz
W8	<b>FEND</b>	Final frequency	MHz
W9	<b>FSTEP</b>	Frequency step	MHz
W10	<b>AZI</b>	Azimuth angle of transmission	rad
W11	<b>AZBEG</b>	Initial azimuth	rad
W12	<b>AZEND</b>	Final azimuth	rad
W13	<b>AZSTEP</b>	Azimuth step	rad
W14	<b>BETA</b>	Elevation angle of transmission	rad
W15	<b>ELBEG</b>	Initial elevation	rad
W16	<b>ELEND</b>	Final elevation	rad
W17	<b>ELSTEP</b>	Elevation step	rad
W20	<b>RCVRH</b>	Height of RX	km
W21	<b>ONLY</b>	Reflected/not reflected rays	0 = only reflected rays 1 = reflected/penetrating rays
W22	<b>HOP</b>	Maximum number of hops	real
W23	<b>MAXSTP</b>	Maximum number of steps for hops	real
W24	<b>PLAT</b>	North geographic latitude of north geomagnetic pole	rad
W25	<b>PLON</b>	East geographic longitude of north geomagnetic pole	rad

**Table 2**

<b>Model</b>	<b>Description</b>	<b>Magnetic Field</b>
<b>Chapman, NF</b>	Analytical electron density profiles	No
<b>Chapman, WF</b>	Analytical electron density profiles	Yes
<b>Discrete, grid, NF</b>	Numerical gridded electron density profiles	No
<b>Discrete, grid, WF</b>	Numerical gridded electron density profiles	Yes



**Computer Code**

[Click here to download Computer Code: Computer Code.doc](#)